Journal of Applied Mechanics and Technical Physics, Vol. 46, No. 5, pp. 677–684, 2005

DYNAMICS OF A GAS BUBBLE DURING ITS INTERACTION WITH COMPRESSION AND RAREFACTION WAVES

D. V. Voronin

UDC 532.529+532.528

The problem of the passage of acoustic waves in the neighborhood of a gas bubble in a tube is formulated and solved numerically. The main parameters determining the bubble dynamics in a nonstationary field are determined. The mechanism of jet deformation of the bubble followed by jet fragmentation and formation of a secondary small-size bubble fraction is studied. A possible explanation of the nature of local sonoluminiscence is proposed.

Key words: *bubbles, shock waves, simulation.*

Introduction. Interest in the wave dynamics of bubbly liquids is motivated by the importance of applying research results to problems of power engineering, gas and oil production industry, and chemical technology. The wave parameters in bubbly media are largely determined by the behavior of a single bubble during its interaction with propagating compression and rarefaction waves. Many theoretical models are based on the assumption that the gas bubble is spherical during oscillations and that the liquid phase is incompressible. In these models, the reverse effect of the pulsating bubble on the external flow is usually ignored (see [1–3]). However, the experiments of Kornfeld and Suvorov [4] revealed that bubbles can collapse asymmetrically with jet formation. Kedrinskii and Soloukhin [5] showed that during compression a bubble gradually loses its spherical shape and becomes convex toward the shock wave (SW) propagation direction. The dynamics of a bubble produced by a laser pulse at a solid boundary was studied experimentally by Vogel et al. [6]. They observed jet formation on the bubble surface even in the initial stages of bubble interaction with strong waves, where the bubble shape should not be significantly distorted by Taylor or Kelvin–Helmholtz instability. They called this phenomenon the jet deformation of bubbles and proposed the following explanation of its mechanism: the nonuniform compression of a bubble gives rise to a liquid cumulative jet, which propagates into the bubble and is then reflected from the opposite wall of the bubble to form a jet directed outward. In addition, local light flashes were recorded inside the bubble near its surface [7]. This implies that the fields of the basic thermodynamic parameters in the bubble can be substantially inhomogeneous. According to modern experiments [3, 8, 9], the action of a strong SW on a single bubble away from a solid wall or on a group of bubbles is also accompanied by jet formation. Consequently, an asymmetric collapse of a bubble can occur when it is located near the boundary with a solid or gas phase or is in a strong SW field.

In modeling asymmetric collapse, it is necessary to take into account the nonstationarity of the external (for the bubble) flow and the reverse effect of the bubble on the liquid under conditions of liquid compressibility. To describe these effects, one needs to solve the complete hydrodynamic equations with explicit interfaces and to calculate the fields of the basic parameters both inside the bubble and in the external liquid flow. It is clear that one-dimensional analysis is insufficient for solving this problem.

The initial stages of interaction of a single bubble with a SW are studied numerically in [10, 11] using the model of two-dimensional unsteady flow of an ideal compressible medium. However, as noted in [3], the deformation of a bubble in the field of strong waves and its effect on the external flow requires further analysis. In the present paper, the interaction of a single bubble with acoustic waves in a bounded volume (tube) is studied numerically.

Lavrent'ev Institute of Hydrodynamics, Siberian Division, Russian Academy of Sciences, Novosibirsk 630090; voron@hydro.nsc.ru. Translated from Prikladnaya Mekhanika i Tekhnicheskaya Fizika, Vol. 46, No. 5, pp. 76–85, September–October, 2005. Original article submitted November 29, 2004; revision submitted December 29, 2004.

Formulation of the Problem. We consider flow in a horizontal tube filled with water at an initial pressure p_0. On the tube axis there is a single gas bubble. Initially, the liquid–bubble system is in dynamic equilibrium and the velocity of the medium is equal to zero. The gas pressure in the bubble is determined from the equilibrium condition taking into account interfacial surface tension. The wave incident on the bubble corresponds to the experimental data of [12] and is a complex which consists of a compression wave and a subsequent rarefaction wave and propagates from the closed left end of the tube. We assume that at the initial time t_0, the wave amplitudes p^* are identical and that the profile is described by half-period of a sinusoid. We denote the initial lengths (at $t = t_0$) of the compression and rarefaction waves by L_1 and L_2. In some papers, such an initial perturbation is called an N-wave [1–3].

After a time, the pulse passes through the bubble and the system enters a state of substantial nonequilibrium with formation of secondary waves. It is assumed that the side walls of the tube are rigid and impenetrable and the right end of the tube is open.

The nature of the pulse, the initial position of the bubble, and the boundary conditions allow the flow to be considered axisymmetric with the symmetry axis coinciding with the tube axis. The coordinate origin is on the symmetry axis at the left end of the tube. The z axis coincides with the tube axis and points along the trajectory of the initiating pulse, and the r axis is normal to the z axis.

The gas bubble dynamics in the liquid is largely determined by losses due to bubble acoustic radiation, viscous energy dissipation, and interfacial surface tension. To estimate the contribution of these factors to the interface velocity, we use the well-known Rayleigh equation, which, according to [3], has the form

$$R\,\frac{dS}{dt} + \frac{3}{2}\,S^2 = \frac{1}{\rho_{01}}\,(\bar{p} - p); \tag{1}$$

$$\bar{p} = p_2 - (4\mu/R + 3\gamma p_2/C_{01})S - 2\alpha/R. \tag{2}$$

Here R and S are the current radius of the bubble and the rate of displacement of its surface, α is the surface tension, μ is the dynamic viscosity of the liquid, ρ_{01} and C_{01} are the density and sound velocity in the liquid, respectively, p_2 is the gas pressure in the bubble, γ is the adiabatic exponent of the gas, and t is time.

Using formulas (1) and (2), one can estimate the ratio of the contributions of viscosity and bubble acoustic radiation to the dissipative losses [the ratio of the terms in the coefficient ahead of S in (2)]:

$$\frac{4\mu C_{01}}{3\gamma R p_2} = \frac{4\mu C_{01}}{3\gamma R_0 p_{02}}\Big(\frac{R}{R_0}\Big)^{3\gamma-1} < \frac{4\mu C_{01}}{3\gamma R_0 p_{02}} = \frac{4}{3\gamma\beta\,\mathrm{Re}},$$

$$\beta = \sqrt{p_{02}/\rho_{02}}\,/C_{01}, \qquad \mathrm{Re} = R_0\rho_{02}\sqrt{p_{02}/\rho_{02}}\,/\mu.$$

Here ρ_{02} is the initial density of the gas and Re is the Reynolds number. Here and below, the subscript 0 refers to the initial state. The last relations imply that for $\beta\,\mathrm{Re} \gg 1$, the energy dissipation due to the viscosity of the liquid phase can be ignored. For the cases studied below, this relation is true. Only for $R_0 \approx 10$ μm do the indicated losses become comparable. Such values of the initial bubble radius are not reached in the model considered. The minimum size of the computational cell used in the calculations is 20 μm. According to (1) and (2), surface tension can have a considerable effect on the bubble dynamics if the interface has a large curvature and moves at a low velocity. The given estimate makes it possible to ignore the losses due to viscosity. This approach is usually employed in modeling the interaction of bubbles with acoustic waves or, for example, in modeling bubble detonation [10, 11].

The flow of a two-phase compressible medium consisting of a liquid and gas bubbles is described by the two-dimensional unsteady Euler equations (of conservation of mass, momentum, and energy) ignoring diffusion and transfer effects:

$$\frac{\partial\boldsymbol{\sigma}}{\partial t} + \frac{\partial\boldsymbol{a}}{\partial z} + \frac{\partial\boldsymbol{b}}{\partial r} = -\frac{1}{r}\,\boldsymbol{f}. \tag{3}$$

For the inert gas inside the bubble, the vector functions $\boldsymbol{\sigma}$, $\boldsymbol{a}$, $\boldsymbol{b}$, and $\boldsymbol{f}$ in system (3) and the total internal energy of the gas E are defined by the relations

$$\boldsymbol{\sigma} = (\rho, \rho u, \rho v, \rho E), \qquad \boldsymbol{a} = (\rho u, \rho u^2 + p, \rho uv, u(\rho E + p)),$$

$$\boldsymbol{b} = (\rho v, \rho uv, \rho v^2 + p, v(\rho E + p)), \qquad \boldsymbol{f} = (\rho v, \rho uv, \rho v^2, v(\rho E + p)), \tag{4}$$

$$E = \frac{1}{\gamma - 1}\,\frac{p}{\rho} + \frac{u^2 + v^2}{2}.$$

Here ρ is the density of the medium, u and v are the velocities in the z and r directions, respectively, and p is the pressure.

For the liquid, the vector functions $\boldsymbol{\sigma}$, $\boldsymbol{a}$, $\boldsymbol{b}$, and $\boldsymbol{f}$ are written as

$$\boldsymbol{\sigma} = (\rho, \rho u, \rho v), \qquad \boldsymbol{a} = (\rho u, \rho u^2 + p, \rho uv),$$
$$\boldsymbol{b} = (\rho v, \rho uv, \rho v^2 + p), \qquad \boldsymbol{f} = (\rho v, \rho uv, \rho v^2). \tag{5}$$

To close system (3), (5), we use the shock adiabat equations for solids or liquids [13]:

$$D = C + LU_*, \qquad \rho(D - U_*) = \rho_0 D, \qquad p = \rho_0 D U_* + p_0, \qquad E = \frac{p + p_0}{2}\Big(\frac{1}{\rho_0} - \frac{1}{\rho}\Big) + E_0. \tag{6}$$

Here D is the shock-wave velocity, U_* is the mass velocity behind the SW front, and L and C are constants. The parameters of the shock adiabat of water were chosen in accordance with the experimental data of [14].

The lower boundary of the computation domain is the symmetry axis of the tube. The nonpenetration condition is imposed on the upper, lower ($v = 0$), and left ($u = 0$) boundaries. The boundary conditions at the right end of the tube correspond to the conditions at the free surface. The interfaces between the liquid and the gas are assumed to be discontinuities. At each of these discontinuities, we specify the boundary continuity conditions for the normal stress-tensor component and the velocity-vector component normal to the surface. The model ignores the effects of gravity, magnetic field, phase transitions, and transfer effects (viscosity, heat conduction, and diffusion). Therefore, the first of these conditions becomes (Laplace formula [15])

$$\Delta p \equiv p_1 - p_2 = \alpha(1/R_1 + 1/R_2), \tag{7}$$

where p_1 and p_2 are the pressures on the opposites sides of the interface and R_1 and R_2 are the major radii of the surface curvature.

The formulated problem with boundary conditions (3)–(7) is solved numerically using the individual particle method [16], which is a modification of the marker-and-cell method (the Harlow method). A nonuniform computational grid with refinement near the symmetry axis was used. The numerical algorithm provides the refinement of the computational grid in high-gradient regions and the possibility of merging and splitting the individual particles belonging to the same body, depending on the current parameters of the medium. The number of particles in the cells is a variable; their maximum number is seven. With time, the gas bubble can deform, split, and merge with other bubbles.

Calculation Results. Let the initial pulse propagate in a channel of diameter $L_0 = 0.004$ m filled with water with an initial density $\rho_{01} = 10^3$ kg/m^3; the wave amplitude is $p* = \pm 11.5$ MPa and $L_1 = L_2 = 0.005$ m. A spherical gas bubble of initial diameter d_0 is suspended in water at the center of the channel. The initial air density in the bubble is $\rho_{02} = 1.225$ kg/m^3, and the surface tension is $\alpha = 0.072$ N/m. The size of the computational domain is $z \times r = 0.035 \times 0.002$ m. At the time $t = 0$, the pulse is at the left boundary of the channel. The Initial coordinates of the center of the bubble are $z = 0.0133$ m and $r = 0$.

The problem in question is a multiparameter one. The main parameters determining the dynamics of processes in the neighborhood of the bubble are as follows: L_1, L_2, p^*, p_0, ρ_{01}, ρ_{02}, L_0, d_0, α, and γ.

In the case of large values of d_0 or high velocities of the interface, where the surface tension has little effect on the bubble dynamics, the problem exhibits geometric similarity. Therefore, we estimate the surface tension. For the initially spherical air bubble in water, the pressure jump in the bubble due to surface tension is $\Delta p \approx 0.15$ MPa for $d_0 = 2$ μm. The dependence $\Delta p(d_0)$ is linear (for example, $\Delta p \approx 0.015$ MPa for $d_0 = 20$ μm). The effect of the surface tension can be considered insignificant for $\Delta p/p^* < 0.01$, which corresponds to values $d_0 > 14$ μm for $p^* = 11.5$ MPa.

The main dimensionless combinations of the initial parameters of the problem

$$\tilde{L} = \frac{L_2}{L_1}, \qquad \tilde{\rho} = \frac{\rho_{01}}{\rho_{02}}, \qquad \tilde{p^*} = \frac{p^*}{p_0}, \qquad \tilde{L}_0 = \frac{L_0}{L_1}, \qquad \tilde{d}_0 = \frac{d_0}{L_1}.$$

The calculations were performed in dimensionless variables. The nondimensionalizing parameters are as follows: $p_0 = 1.01 \cdot 10^5$ Pa, $\rho_{02} = 1.225$ kg/m^3, $u_0 \equiv \sqrt{p_0/\rho_{02}} = 287.6$ m/sec, and $t_0 \equiv L_1/u_0 = 1.739 \cdot 10^{-5}$ sec.

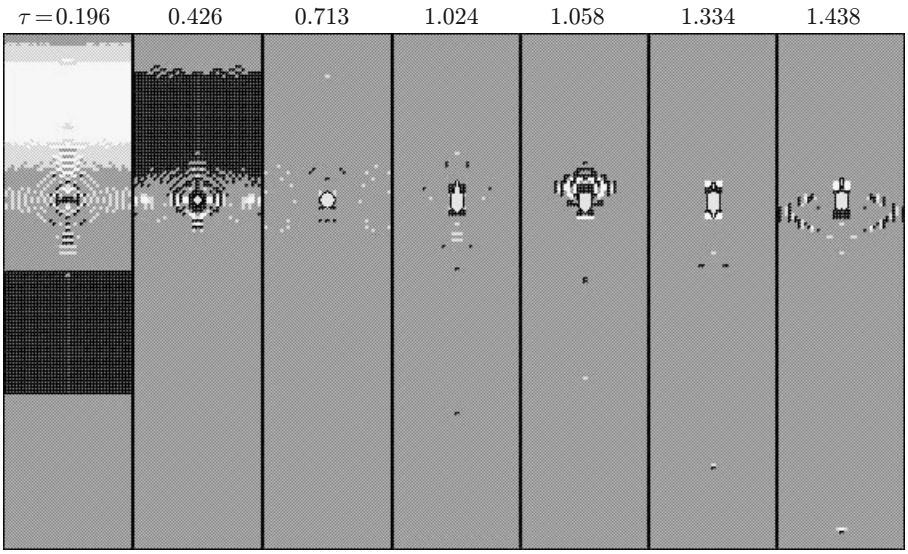

Fig. 1. Formation of a bubble in an acoustic wave.

Experiments have shown that in the initial stages of formation of a bubble cluster, the bubble diameter distribution has a bimodal nature: there are two fractions with greatly different bubble sizes [9, 17]. To find the reason for this, we consider the dynamics of bubble formation from a cavitation nucleus during motion of the above-mentioned pulse in water with a single microbubble. A single microbubble of diameter $d_0 = 40$ μm (in dimensionless variables, $\tilde{d}_0 = 0.008$) is placed on the symmetry axis at the center of the tube. Because the bubble is small compared to the characteristic geometrical dimensions of the problem, the energy of the initial pulse varies only slightly during motion through the neighborhood of the bubble. The interaction of the microbubble with the initial pulse is presented in Fig. 1, which shows a background picture of the pressure field in the neighborhood of the bubble. The lighter color in the figure corresponds to compression waves ($\tilde{p}^*_{\max} = 115$), and the darker color to rarefaction waves ($\tilde{p}^*_{\min} = -115$). Time is reckoned ($\tau = t/t_0$) from the moment the initial compression wave reaches the neighborhood of the bubble. In Fig. 1, the pulse moves from bottom to top. In the first frame, the microbubble remains invisible and appears only by the time $\tau = 0.426$ when a rarefaction wave passes. In the initial stage, quasispherical growth of the bubble is observed. By the time $\tau = 0.713$, its diameter reaches the value $\tilde{d}_0 = 0.114$. The growth is accompanied by the formation of a secondary quasispherical compression wave, which diverges from the bubble. Upon reflection from channel walls, it again reaches the neighborhood of the bubble; therefore, its further expansion is accompanied by a considerable shape distortion. The cross-sectional diameter decreases to 0.068, and a jet pointing along the trajectory of the N-wave is formed on the upper boundary of the bubble. The maximum length of the jet (at $\tau = 1.035$) is comparable with the average bubble diameter.

In the interval $1.04 < \tau < 1.05$, the pulsation flow of the liquid leads to a rapid decrease in the cross-sectional diameter of the jet to a size smaller than the size of the computational cell, which physically corresponds to the collapse of the jet. At subsequent times, a similar jet begins to form on the opposite side of the bubble. During the collapse, the jet undergoes fragmentation, resulting in the formation of a new small bubble. The bubble becomes visible by the time $\tau = 1.173$, and its longitudinal diameter reaches 0.02 at $\tau = 1.438$. The dynamics of the jet from the lower side of the bubble is similar. Its collapse and fragmentation occur by the time $\tau = 1.392$, after which expansion and formation of a daughter bubble take place. The formation of a similar structure with one large bubble and two small bubbles located on both sides of the large bubble along the trajectory of the initial pulse is confirmed by the experimental data of [17].

Thus, the passage of the indicated acoustic pulse through a cavitation nucleus is accompanied by the formation of a rather large bubble, its jet deformation with the subsequent collapse and fragmentation of the jet, and the formation of daughter bubbles. A similar mechanism may be responsible for the formation of bubble clusters with a bimodal distribution in the initial stages of motion of strong waves in liquids.

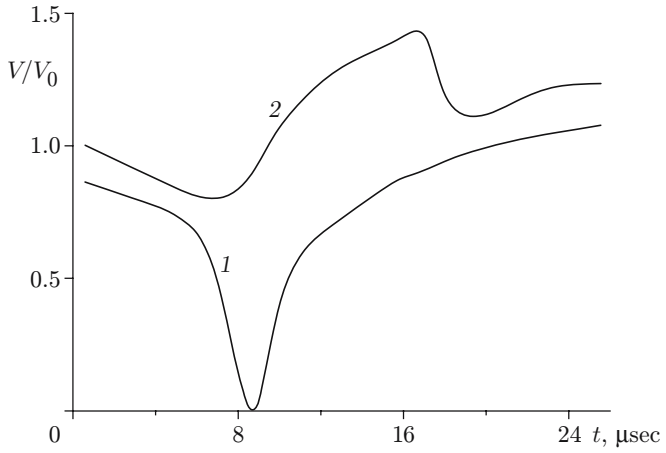

Fig. 2. Bubble diameter versus time: $d_0 = 700$ (1) and 740 μm (2).

Let us consider the interaction of a rather large bubble with the initial pulse. Figure 2 gives the dynamics of the bubble volume in the acoustic wave (V_0 is the initial volume of the second bubble). It is evident that the dynamics of the bubbles is significantly different. Calculations show that for the fixed parameters of the incident pulse there is the critical diameter $d_0 \approx 730$ μm, for which the bubble behavior in the wave changes significantly: for $d < d_0$, the bubble collapses in the incident wave, and for $d > d_0$ there is no collapse. The collapse and jet deformation of the bubbles occur in this case because of a rapid change in the liquid pressure and velocity fields in the wave incident on the bubble. The bubble deformation can involve different mechanisms, such as the development of Taylor and Kelvin–Helmholtz instabilities at the interface for Bond and Weber numbers higher than the critical values. From the calculations it follows that for a bubble diameter $d_0 = 200$ μm in the wave described above (with $L_1 = 0.005$ m), pronounced jet deformation occurs by the time $t = 20$ μsec, whereas the minimum time of development of the above-mentioned instabilities in this case is approximately 120 μsec. The existence of the critical diameter is supported by experimental data on pulse propagation in bubble clusters [9]. The somewhat smaller value of the critical diameter in experiments is explained by the mutual interaction of bubbles, which promotes their greater deformation.

Figure 3 shows the pressure field at the time $\tau = 0.322$ for $d_0 = 700$ μm ($\tilde{d}_0 = 0.14$). Fig. 3a gives a background picture of the pressure field (the wave moves from left to right); Fig. 3b and Fig. 3c give the pressure profiles in the cross and longitudinal sections indicated in Fig. 3a by dashed lines. By this time, the compression wave has passed through the bubble with an insignificant change in its amplitude. As is evident from the figure, collapse of the bubble began. The bubble decreases in size, and the gas pressure inside the bubble grows (wave A in Fig. 3c), far exceeding the amplitude of the initial pulse in the compression wave. A rarefaction wave has not yet passed through the bubble. We note that the bubble collapse is a nonspherical process. At the left boundary of the bubble, the pressure is higher and the velocity of the medium on the symmetry axis is $u = 0.522$ at that time. At the opposite right boundary, $u = -0.104$. The nonsphericity of the bubble compression leads to the formation of a cumulative water jet at the left boundary of the bubble, which is directed into the bubble (Fig. 3a). In this case, the maximum velocity of the interface reaches the value $u = 0.904$. We note that the velocity of the jet depends on the steepness of the compression-wave profile with its unchanged length and amplitude. The steeper the profile, the more pronounced the jet.

At subsequent times, the average bubble diameter decreases rapidly to the size of the computational cell. In the expansion stage ($\tau > 0.5$), a compression wave is formed around the bubble; the amplitude of this wave is similar in order of magnitude to the amplitude of the initial compression wave. A fundamental condition for the formation of a powerful secondary wave suffices is the preliminary collapse of the bubble. For $\tilde{d}_0 > \tilde{d}_0^*$, the intensity of the secondary compression wave is low.

Next, we consider the dynamics of a rather large bubble with an initial diameter $d_0 = 0.001$ m ($\tilde{d}_0 = 0.2$) under the same initial conditions (Fig. 4). By the time $\tau = 0.253$, the total volume of the bubble is about 51% of

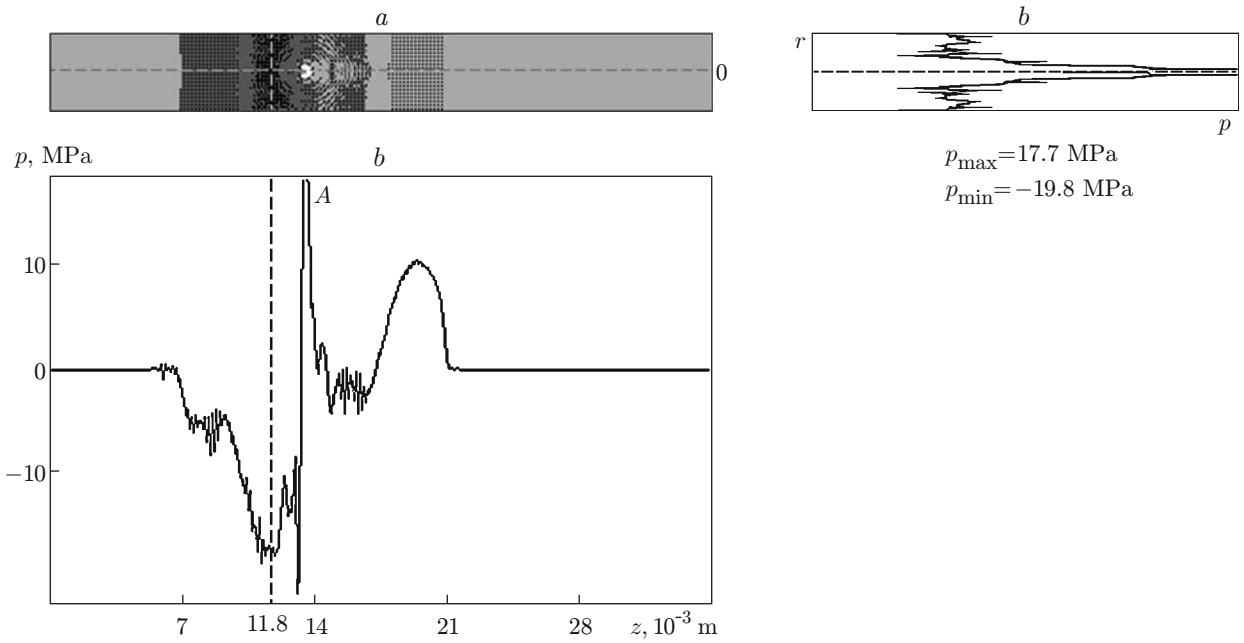

Fig. 3. Pressure profiles at the time $\tau = 0.322$: background picture of the pressure field (a), in cross section (b), and in longitudinal section (c).

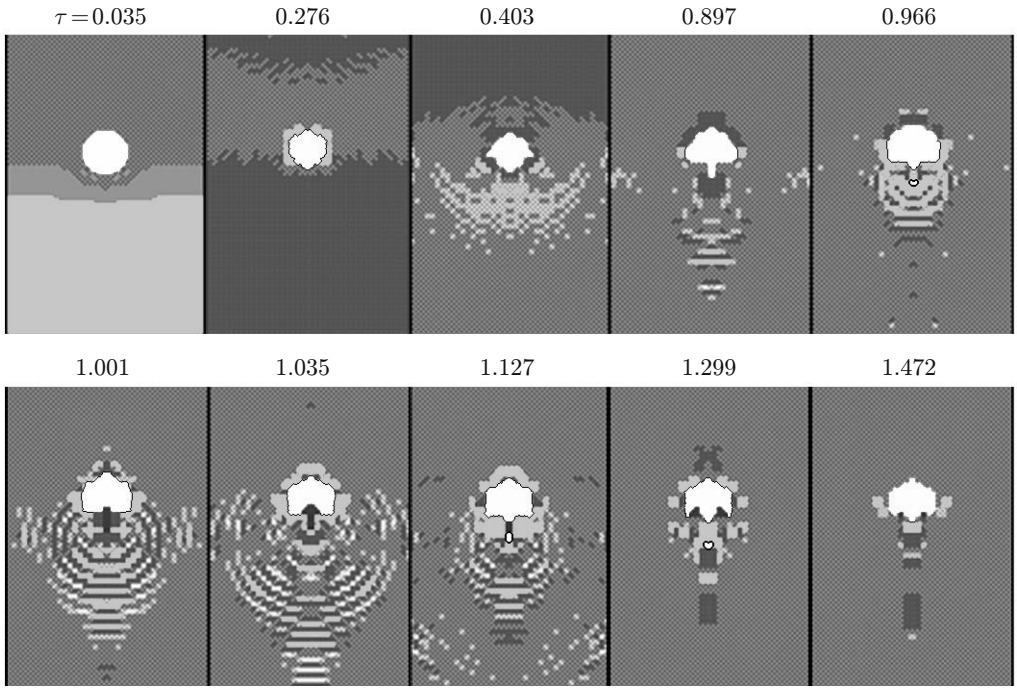

Fig. 4. Fragmentation of a large bubble in an acoustic wave.

the initial volume (the effect of the compression phase of the initial wave). In Fig. 4, the pulse moves from bottom to top. The compression process is nonspherical. As in the previous case, the bubble is more deformed on the side facing the incident wave. The compression wave profile is flat enough; therefore, the cumulative water jet directed into the bubble is less pronounced than that in Fig. 3. In this case, complete collapse of the bubble in the incident wave does not occur because the initial diameter of the bubble exceeds the critical value $\tilde{d}_0^* = 0.146$. By the time

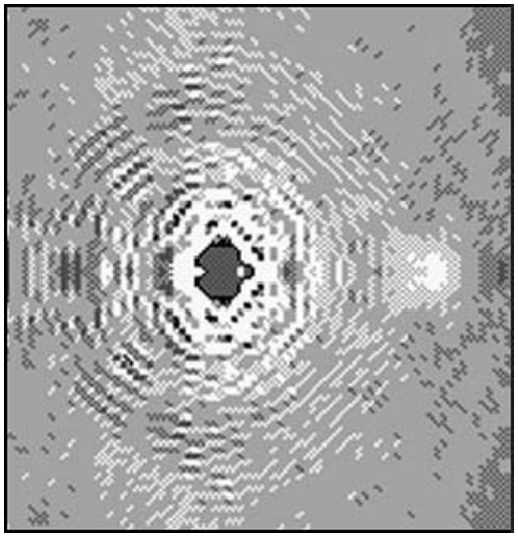

Fig. 5

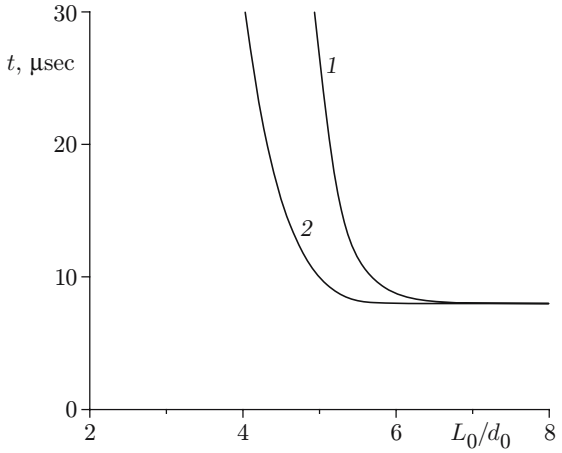

Fig. 6

Fig. 5. Deformation of a bubble by a water jet.

Fig. 6. Bubble collapse time versus tube diameter: $\tilde{p}* = 115$ (1) and 230 (2).

$\tau = 0.897$, a gas jet (a tip) is formed on the bubble surface facing the incoming rarefaction wave. Collapse of the jet occurs by the time $\tau = 1.001$ and is accompanied by the fragmentation of the tip ($\tau = 0.966$). The resulting fragment begins to oscillate in the acoustic field of the large bubble, reaching the largest average diameter of 0.027 at $\tau = 1.127$ and collapsing at $\tau = 1.035$ and 1.472. During the oscillations, the distance between the bubbles increases and the small bubble migrates from the large bubble at a velocity reaching 0.278. Consequently, the pulsation flow of the liquid in the neighborhood of the bubble generates bubbles of much smaller sizes, and bubble clusters with bimodal distributions are formed during interaction of the initial disturbance with the already existing large bubbles.

The velocity of the bubble boundary is determined by the amplitude of the incident waves and the pressure gradient in it. These parameters affect the dynamics of the cumulative water jet directed into the bubble. This jet can lead to complete failure of the bubble and collapse of its fragments at $\tilde{d}_0 < \tilde{d}_0^*$. In the transition zone, the jet reaches the opposite wall of the bubble, and the bubble shape thus becomes toroidal. In addition, the jet can stop without reaching the other wall of the bubble because of the pulsation liquid flow due to the passage of a strong rarefaction wave in the neighborhood of the bubble (Fig. 5). In this case, a convergent SW moves in the gas inside the bubble. The focusing of this wave (the light region at the right boundary of the bubble in Fig. 5) leads to a considerable increase in the local thermodynamic parameters of the gas. Calculations show that in this case and in the period of jet collapse, the local pressure can increase to 0.8 GPa and the gas temperature to 11,000 K. This effect should be accompanied by radiation from the gas in the local region with the indicated thermodynamic parameters, which suggests that a similar mechanism may be responsible for the nature of local luminescence (the formation of luminous spots at the bubble surface) observed in the experiments of [18]. The subsequent interaction of the bubble with the initial rarefaction wave (Fig. 5) results in the formation of a gas jet directed toward this wave, as in Fig. 4.

From the calculations it follows that the jet deformation of a single bubble in the initial stages of its interaction with acoustic waves of large amplitude, where Taylor or Kelvin–Helmholtz instability has not yet developed, is due primarily to the closeness of the rigid boundary (the tube wall) and the nonuniformity of the incident-wave profile. Figure 6 gives calculated times of bubble collapse versus the dimensionless parameter $\lambda = L_0/d_0$. For $\lambda > 7.5$, the bubble size decreases rapidly in the incident wave while its shape remains almost spherical. As λ decreases, the jet deformation becomes more pronounced. For $\lambda < 4.5$ and $\tilde{p}* = 115$ and for $\lambda < 3.7$ and $\tilde{p}* = 230$, the bubble deforms without collapse. During bubble collapse, the maximum velocity of the interface can reach $u \approx 1.86$. These results are in good agreement with the experimental data of [8].

Conclusions. Thus, the present study showed that the interaction of a single bubble with an acoustic wave in a tube gives rise to secondary compression waves (with an amplitude comparable to the initial wave) in two cases: if the initial compression wave provides a collapse of the bubble and if the tensile stress in the rarefaction wave exceeds the surface tension and a bubble originates from the cavitation nucleus. The determining parameter for the formation of secondary waves is the ratio of the initial bubble diameter to the incident-wave length $\tilde{d}_0$. When $\tilde{d}_0$ is larger than the critical value, bubble collapse does not occur. In the transition region, there is jet deformation of the bubble with the subsequent jet fragmentation, which may be responsible for the formation of the bimodal cluster observed in experiments. The transition from quasispherical collapse to jet deformation is also determined by the ratio of the channel diameter to the initial diameter of the bubble. The jet fragmentation is accompanied by a considerable increase in the local values of the thermodynamic parameters, which may be responsible for the luminescence in local regions near the interface.

This work was supported by the Russian Foundation for Basic Research (Grant No. 03-02-17682a) and the Integration Project No. 123 of the Siberian Division of the Russian Academy of Sciences.

REFERENCES

1. S. S. Kutateladze and V. E. Nakoryakov, *Heat and Mass Transfer and Waves in Gas–Liquid Systems* [in Russian], Nauka, Novosibirsk (1984).
2. R. I. Nigmatulin, *Dynamics of Multiphase Media*, Parts 1 and 2, Hemisphere, New York (1991).
3. V. K. Kedrinskii, *Detonation Hydrodynamics: Experiment and Models* [in Russian], Izd. Sib. Otd. Ross. Akad. Nauk Novosibirsk (2000).
4. M. Kornfeld and L. Suvorov, "On the destructive action of cavitation," *J. Appl. Phys.*, **15**, 495–506 (1944).
5. V. K. Kedrinskii and R. I. Soloukhin, "Shock wave compression of a spherical gas cavity in water," *Zh. Prikl. Mekh. Tekh. Fiz.*, No. 1, 27–29 (1961).
6. A. Vogel, W. Lauterborn, and R. Timm, "Optical and acoustic investigation of the dynamics of laser-produced cavitating bubbles near a solid boundary," *J. Fluid Mech.*, **206**, 299–338 (1989).
7. W. Lauterborn, T. Kurz, R. Mettin, and C.-D. Ohl, "Experimental and theoretical bubble dynamics," *Adv. Chem. Phys.*, **110**, 295–380 (1999).
8. V. S. Teslenko, "Experimental investigation of the kinetic energy singularities of a collapsing bubble from laser breakdown in a viscous liquid," *J. Appl. Mech. Tech. Phys.*, No. 4, 543–549 (1976).
9. D. V. Voronin, G. N. Sankin, V. S. Teslenko, et al., "Secondary acoustic waves in a polydisperse bubbly medium," *J. Appl. Mech. Tech. Phys.*, **44**, No. 1, 17–26 (2003).
10. F. N. Zamaraev V. K. Kedrinskii, and C. Mader, "Waves in a chemically active bubbled medium," *J. Appl. Mech. Tech. Phys.*, No. 2, 179–184 (1990).
11. Z. Ding and S. M. Gracewski, "The behavior of a gas cavity impacted by a weak or strong shock wave," *J. Fluid Mech.*, **309**, 183–210 (1996).
12. D. V. Voronin, G. N. Sankin, and V. S. Teslenko, "Modeling secondary shock waves under cavitation conditions," in: *Physical Acoustics and Wave Propagation and Diffraction*, Proc. of the XI session of the Russian Acoustic Society, Vol. 1, Moscow (2001), pp. 175–179.
13. R. Kinslow (ed.), *High-Velocity Shock Phenomena*, Acad. Press, New York–London (1970).
14. R. F. Trunin, "Compression of condensed materials by high shock-wave pressures (laboratory research)," *Usp. Fiz. Nauk*, **171**, No. 4, 387–414 (2001).
15. L. D. Landau and E. M. Lifshits, *Course of Theoretical Physics*, Vol. 6: *Fluid Mechanics*, Pergamon Press, Oxford-Elmsford, New York (1987).
16. V. A. Agureikin and B. P. Kryukov, "Method of individual particles for calculating flows of multicomponent media with large strains," in: *Numerical Methods of Continuum Mechanics* (collected scientific papers) [in Russian], Inst. of Theor. and Appl. Mech., Sib. Div., Acad. of Sci. of the USSR, Vol. 17, No. 1 (1986), pp. 17–31.
17. D. V. Voronin, G. N. Sankin, and V. S. Teslenko, "Generation and dynamics of bubble cluster following an acoustic pulse," in: *Proc. of the 5th World Congress on Ultrasonics* (WCU 2003), Paris, France, Sept. 7–10 (2003), pp. 116.
18. J. P. Dear, J. E. Field, and A. J. Walton, "Gas compression and jet formation in cavities collapsed by a shock wave," *Nature*, **332**, 505–508 (1988).